Volume 1 | Number 1 | Jan 2013 | Pages 1–100

Catalysis
Science &
Technology

www.rsc.org/catalysis

ROYAL SOCIETY
OF CHEMISTRY

ROYAL SOCIETY
OF CHEMISTRY

www.rsc.org/catalysis

Catalysis Science & Technology

PAPER

Hydrogen production by ammonia decomposition using high surface area Mo_2N and Co_3Mo_3N catalysts

Seetharamulu Podila[a], Sharif F. Zaman[a,b]*, Hafedh Driss[b], Yahia A. Alhamed[a,b], Abdulrahim A. Al-Zahrani [b], Lachezar A. Petrov[a]

High surface area, bulk molybdenum nitride catalysts were synthesized via temperature programmed ammonalysis of ammonium hepta molybdate and citric acid (CA) composite. The sythesized materials were tested for COx free H_2 production via ammonia decomposition for fuel cell application. Cobalt was added in different loadings (1, 3, 5wt %) as a promoter for the bulk molybdenum nitrides. The chemical composition and surface morphology of nitride catalysts were studied by XRD, XPS, SEM-EDAX and TEM techniques. Addition of cobalt increased the formation of γ-Mo_2N phase and cobalt existed as Co_3Mo_3N phase, which was uniformly distributed over Mo_2N evidenced by TEM and SEM analysis. A drastic increase in Mo_2N crystal size was observed when the Co loading exceeded 3 wt%, which in turn decreased the catalyst activity for ammonia decomposition reaction. All catalysts are exhibiting high activity than reported nitride catalysts at low temperatures. All catalysts showed stable activity for 30 hours. Activation energy calculated for ammonia decomposition was decreased drastically from 131.2 to 99kJ/mol by the addition of cobalt (1 wt%) in Mo_2N prepartion.

[a.] SABIC Chair of Catalysis, King Abdulaziz University, P.O. Box 80204, Jeddah 21589, Saudi Arabia. Email: seetharampodila@gmail.com

[b.] Chemical and Materials Engineering Department, Faculty of Engineering, King Abdulaziz University, P.O. Box 80204, Jeddah 21589, Saudi Arabia.
Email: sfzaman@kau.edu.sa , zfsharif@gmail.com;
Tel: +966 563063594

1. Introduction

Ammonia is very important hydrogen storage medium. Hydrogen produced by catalytic ammonia decomposition does not contain carbon monoxide or other catalytic poisons. For that reason, its use in fuel cells for energy production has very good prospects.

Compared with all organic compounds ammonia has the highest hydrogen content of 17.75 wt.%. It is non-flammable and non-explosive. Ammonia liquefaction takes place under mild conditions at about 10 bars at room temperature.[1] The reaction of ammonia decomposition can easily be realised in practice. Thermodynamic calculations show that at a pressure of 1 atm. It is possible to achieve a 99% ammonia conversion at 400°C. [2,3]

Many transition and noble metals (Ru, Fe, Co, Ni, Ir, and Rh) have been tested as catalysts for ammonia decomposition.[3,4,5,6] It was found that the most active catalyst was ruthenium supported on multi-walled carbon nanotubes (MWCNTs).[7] However, some studies reported that carbon nano fibers and MgO-CNTs composite are better support than CNTs for Ru system.[8,9] Unfortunately, this metal is scarcely available and, besides, many non-precious metals are known as low active catalysts without being promising for future commercial use. Thus, it is necessary to design and develop new catalytic systems based on non-precious metals that exhibit high activity at low temperatures.

Transition metal nitrides belong to a class of interstitial compounds, in which nitrogen atoms replace oxygen atoms in the metal oxide crystal structure. Owing to their similarity with group VIII noble metals, these materials have attracted much attention as potential catalysts for many reactions.[10–12] It is well-known that the metal-nitrogen interaction plays an important role in both the synthesis and decomposition of ammonia, since nitrogen adsorption and nitrogen desorption are the rate-limiting steps of ammonia synthesis and ammonia decomposition, respectively.[12-16] Reference studies of molybdenum nitride preparation claim that ammonalysis under programmable controlled heating is the best route to obtain a high surface area product.[17–20] Volpe et al.[18] have prepared high surface area Mo_2N from molybdena, MoO_3. Other published reports deal with molybdenum nitride synthesis from different precursors; however, the prepared samples do not expose substantially higher surface areas than those reported by Vople.[21]

In recent years, ternary nitride systems have attracted considerable attention for catalytic application and especially for ammonia synthesis.[22–26] Low-priced unsupported non-precious metal-based catalysts are very attractive for ammonia decomposition. So far, few studies have been published on the application of Mo_2N and cobalt-molybdenum nitride for production of CO_x-free hydrogen through ammonia

decomposition. However, all the reported catalysts have exhibited a moderate activity at high temperatures.[27–33]

Consequently, our aim in this investigation is to develop a new method for preparation of high surface area unsupported molybdenum nitride. This method used ammonalysis to add citric acid to precursor salt(s). After nitridation the obtained material was examined for its catalytic activity in ammonia decomposition. Mo_2N activity in the presence of cobalt was also being investigated. Catalytic activity results were correlated to the morphological, chemical, and structural characteristics of the prepared materials. These materials were characterised by means of the following techniques: BET, XRD, TPR, XPS, SEM, and TEM analysis.

2. Experimental

Catalyst preparation

A high surface area Mo_2N catalyst was prepared by dissolving a calculated amount of ammonium heptamolybdate ($(NH_4)_6Mo_7O_{24}.4H_2O$) in 30 cm^3 of deionized water. Citric acid (CA) was dissolved in 30 cm^3 of deionized water and added to the Mo salt solution to obtain a CA to Mo molar ratio of 1:1. After introduction of CA, the precursor solution was aged for 24 h in a beaker held at 90°C in a water bath followed by drying in an oven at 110°C for 24 h. The dried catalyst was ground to a powder and calcined at 500°C for 5 h in stagnant air. This temperature was established by a ramping rate of 5°C min^{-1}. Then nitridation was performed in a packed bed under pure ammonia flow. The temperature was increased up to 700°C by a ramping rate of 0.5°C min^{-1}.[18] After nitridation and before exposing to air, the catalyst was pretreated with helium containing 1 vol.% O_2 for 2 h at room temperature. This catalyst was denoted as MoN. Cobalt containing catalysts were prepared by adding required amount of cobalt nitrate to ammonium heptamolybdate solution. This is followed by addition of citric acid and the remaining procedure is same as described above. The amount of added cobalt salt was selected to give 1, 3, and 5 wt.% content of Co. The cobalt containing catalysts were designated as 1CoMoN, 3CoMoN, and 5CoMoN, respectively. All chemical reagents used in this study were supplied by Aldrich chemicals.

Catalytic activity measurements

Catalytic activity tests were performed at atmospheric pressure in a PID Eng&Tech system (Spain) by a fixed bed quartz reactor with external diameter of 6.0 mm. The reactor was charged with 0.1 g catalyst. Prior to reaction, the catalyst was activated at 500°C in nitrogen flow for 1 h. Reduction with hydrogen flow followed then for 5 h and flushing again with N_2 for 1 h at the same temperature. After the catalyst activation, the reactor temperature was decreased down to

300°C and a pure ammonia gas was introduced into the reactor at a GHSV of 6000 h^{-1}. Then the temperature was increased stepwise by 50°C. At each temperature, the reaction was conducted until a steady state regime was established. A steady state was verified by a relative percentage difference less than 5% for two successive runs of effluent gas analysis. The catalytic experiments were carried out at temperatures within the range of 300–600°C. Effluent gas analysis was performed by an online-connected gas chromatograph (GC-450 Varian, USA) equipped with a thermal conductivity detector and a Poropak Q column.

Catalyst characterisation

The BET surface area of the catalysts was determined by N_2 physisorption at -196°C using a Quantachrome Nova2000 Win2 apparatus. Before measurements, the samples were degassed at 300°C for 3 h.

X-ray diffraction (XRD) was performed using an Inel Equinox 1000 powder diffractometer equipped with a CPS 180 detector (filtered Co Kα1 radiation, 40 kV, 30 mA, spinning sample holder). Powder pattern analyses were processed using Match© Crystal Impact software (v.1.11e) for phase identification (using both COD and ICSD databases), IMAD-INEL© XRD software (v.4.8) for graphical illustrations and MAUD© software for Rietveld analysis. All the data were collected under the same conditions.

XPS measurements were carried out in a Specs GmbH high vacuum multi-technique surface analysis system equipped with an Mg-Kα 1253.6 eV X-ray source. As a common practice in XPS studies, the adventitious hydrocarbon C 1s line (284.8 eV) corresponding to a C–C bond was used as a binding energy reference for charge correction.

Sample morphology was investigated by means of field emission scanning electron microscopy (FE-SEM, Quanta FEG450, FEI) using an ETD Everhart Thornley detector (HV mode) and a solid-state back scattering electron detector (VCD).

TEM analysis of all the catalyst samples was performed using a Tecnai G2 F20 Super Twin device at 200 kV with a LaB6 emitter. The microscope was fully equipped for analytical work with an energy-dispersive X-ray (EDX) detector with an S-UTW window and a high angle annular dark-field (HAADF) detector for STEM imaging. Unless stated otherwise, the scanning transmission electron microscopy (STEM) imaging and all analytical work were performed with a probe size of 1 nm^2 resulting in a beam current of about 0.5 nA. TEM images and selected area diffraction (SAD) patterns were collected on an Eagle 2K HR 200kV CCD camera. The HAADF-STEM EDX and CCD line traces were collected fully automatically using the Tecnai G2 User Interface and processed with the Tecnai Imaging and Analysis (TIA) software Version 1.9.162.

Journal Name

ARTICLE

Table 1 BET surface area and average particle crystallites size of the studied catalysts

Catalyst	BET surface area m^{2}g^{-1}		Average particle size of γ-Mo$_2$N^a nm	Average crystallite size of γ-Mo$_2$N^b nm	Average crystallite size of ^{b}MoO$_2$ nm	Average crystallite size of ^{b}Co$_3$Mo$_3$N nm	Relative proportional weight^c, %		
	Fresh	Used					MoO$_2$	Mo$_2$N	Co$_3$Mo$_3$N
MoN	110	78	7	7	169	–	54	46	–
1CoMoN	91	65	11	12	98	8	27	71	2
3CoMon	93	71	9	10	100	14	20	76	4
5CoMoN	83	59	23	13	110	20	3	90	7

^{a} Particle size calculated from TEM analysis
^{b} Crystal size calculated from XRD using Rietveld refinement analysis
^{c} Relative proportional weight (%) calculated from XRD using Rietveld refinement analysis

3. Results and discussion

To the best of our knowledge, so far high surface area molybdenum nitride has been prepared by using pure MoO$_3$ as a starting material.[17,18] Jaggers et al.[18] have obtained molybdenum nitride from ammonium heptamolybdate and reported a surface area of 57 m^{2}g^{-1}. By applying the method described above a sample of higher surface area, 110 m^{2}g^{-1}, was prepared (see Table 1), this value being considerably higher than that reported by Jaggers et al.[21] The result is probably due to Mo citrate formation during the catalyst preparation procedure. Likely, on calcination the presence of molybdenum citrate prevents metal crystallite agglomeration. Table 1 clearly shows that adding different amounts of cobalt (1, 3, 5 wt.%) during molybdenum nitride preparation did not induce any significant changes of sample surface area.

This finding explains why no significant structural transformations occurred in the Mo$_2$N catalysts on increasing Co amount (1, 3, 5 wt.%). Results of the physical and structural characterisation of the molybdenum nitride and cobalt/molybdenum nitride catalysts are summarised in Table 1.

The pore size distribution patterns of all fresh catalysts are presented in the supplementary information (**Fig.S1**). The pore size distribution patterns revealed the existence of pores in micro and meso range for all catalysts. Addition of cobalt in Mo$_2$N preparation mesoporosity was increased (increased pores in meso range **Fig.S1**). This might be due to the dispersion of formed Co$_3$Mo$_3$N phase on Mo$_2$N platelets. The increase in Co loading from 1-3%, mesoporosity was increased, indicating increase in the distribution of Co$_3$Mo$_3$N phase. Further increase in cobalt loading upto 5% mesoporosity was decreased. This might be due to agglomeration of Co$_3$Mo$_3$N and Mo$_2$N phases. The

surface area results of used catalysts are also displayed in Table 1. These results indicate a decrease in specific surface area for used catalysts compared to that of fresh catalysts. The decrease in surface area of used catalysts is due to oxidation of catalyst by exposing it to air after reaction. For the fresh catalysts we passivated the catalysts with 1%O_2 in He at room temperature after nitridation prior to exposing the catalysts to air which helps to retain the high surface area of fresh catalysts.

X-ray diffraction analysis

Figure 1 displays XRD patterns of molybdenum nitride as well of the 1CoMoN, 3CoMoN, and 5CoMoN cobalt molybdenum nitrides. The diffractogram of the MoN sample shows mainly the presence of γ-Mo_2N [ICSD No. 158843] and MoO_2 [ICSD No. 80830] phases. In the cobalt molybdenum nitride catalysts, Co_3Mo_3N [ICSD No.

Fig. 1 X-ray diffraction patterns of MoN, 1CoMoN, 3CoMoN, and 5CoMoN catalysts.

180409], Mo_2N and MoO_2 phases are detected. Figure 1 indicates that on increasing Co amount in the cobalt molybdenum nitride samples an increase in Co_3Mo_3N phase and a decrease in MoO_2 phase took place. The average crystallite size of the different phases and their relative weight percentage calculated from XRD using Rietveld refinement analysis are shown in Table 1. From these data, it follows that the MoN catalyst consists of two phases: γ-Mo_2N (46%) and MoO_2 (54%). Introduction of 1 wt.% Co to MoN leads to a drastic increase in content of the γ-Mo_2N phase from 46 to 71% and, at the same time, formation of a Co_3Mo_3N phase is also observed. On increasing Co loading from 1 to 3 wt.% a further increase in content of both the γ-Mo_2N and Co_3Mo_3N phases is observed. An additional increase in Co loading up to 5 wt.% does not lead to an extra increase of the γ-Mo_2N phase. It seems that the amount of the latter phase reaches a maximum for these conditions. In addition, a growth of the Co_3Mo_3N phase is observed under the same conditions. For a 5% Co loading, we also detected amorphous cobalt oxide by TEM-EDX analysis. Concerning γ-Mo_2N phase amount we noticed that the difference between the MoN and 1CoMoN catalysts is higher in comparison with the difference among the 1CoMoN, 3CoMoN, and 5CoMoN catalysts. This indicates that cobalt introduction is promoting the formation of both γ-Mo_2N and Co_3Mo_3N phases simultaneously.

This statement is supported by inspecting both the crystal size (Table 1) and XRD signal intensity (Fig. 1) of the MoO_2 phase. The effect of cobalt introduction to the molybdenum nitride has specific features: (i) the intensity of the Mo_2N signal is substantially increased and (ii) this increase is not strongly dependent on Co concentration. The details of Rietveld refinement analysis of 5CoMoN sample were presented in the supplementary information (**Fig.S2**). Similar procedure was adopted to analyze other catalysts. Hada et al.[34] detected insignificant amount of Co_3Mo_3N formation in nitridation of 25% Co and 75%Mo at 700°C. He detected the beginning of a

Co_3Mo_3N phase on increasing cobalt amount up to 50%. Similarly, other researchers have reported the preparation of Co_3Mo_3N on different supports. They also detect formation of a Co_3Mo_3N phase at higher Co loadings.[27–30] One can draw a conclusion on examining Figure 1 that the formation of a Co_3Mo_3N phase takes place because of the addition of cobalt to the MoN preparation. This is due to formation of bimetallic (CoMo) complex with citric acid during catalyst preparation. The existence of the bimetallic complex ensures the formation of the oxide precursors with close proximity between Co and Mo during calcinations.[35] These consequences provides the
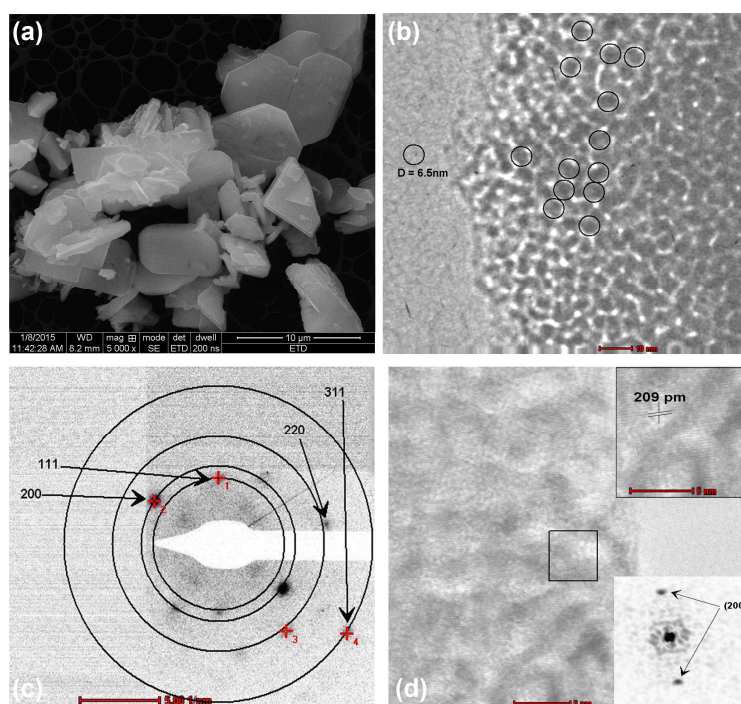
Fig. 2 (a) SEM of a MoN sample; (b) HRTEM of γ-Mo_2N; (c) selected-area electron diffraction pattern of a γ-Mo_2N platelet; (d) HRTEM of γ-Mo_2N and corresponding SAED.

formation of highly disperse nitride particles during nitridation step. This explains the role of citric acid in catalyst preparation. This chelating agent helps in controlling metal agglomeration during high temperature calcinations.[35] A comparison study of X-ray diffraction analysis of fresh, reduced and used 3CoMoN catalyst is displayed in the supplementary information **Fig.S3**. The results indicated an increase in crystal size in reduced and spent catalysts referred on the basis of peak intensities. The crystal growth was majorly observed in MoO_2 phase in comparison with γ-Mo_2N phase. The bulk structure of γ-Mo_2N was retained and no other new phases were observed in the reduced and used catalysts in comparison with the fresh catalyst. This observation indicates a high stability of γ-Mo_2N phase during ammonia decomposition process. Tagliazucca et al. [36] reported that molybdenum nitride catalyst showed structure variations with the increase in temperature during ammonia decomposition process by observing a shift of X-ray reflection to higher 2θ values at higher temperatures. However we didn't observe any shift in 2θ values for X-ray reflection for used catalysts, but observed relative increase of crystalline MoO_2 phase. This may be due to the oxidation of catalyst by exposing it to air after the reaction.

SEM and TEM studies

Sample morphologies were investigated by scanning electron microscopy (SEM) and transmission electron microscopy (TEM). Representative SEM and TEM images of a MoN sample are shown in Figure 2. Because the nitriding process is topotactic, Mo_2N is formed in a pseudo amorphous platelet's form. MoO_2 is also formed along with γ-Mo_2N and occurs in the form of large crystallites, which are clearly seen in Fig. 2a. These results show a good correlation with XRD measurements where a very sharp narrow MoO_2 peak with the MoN sample is observed. As per literature reports, MoO_2 undergoes no
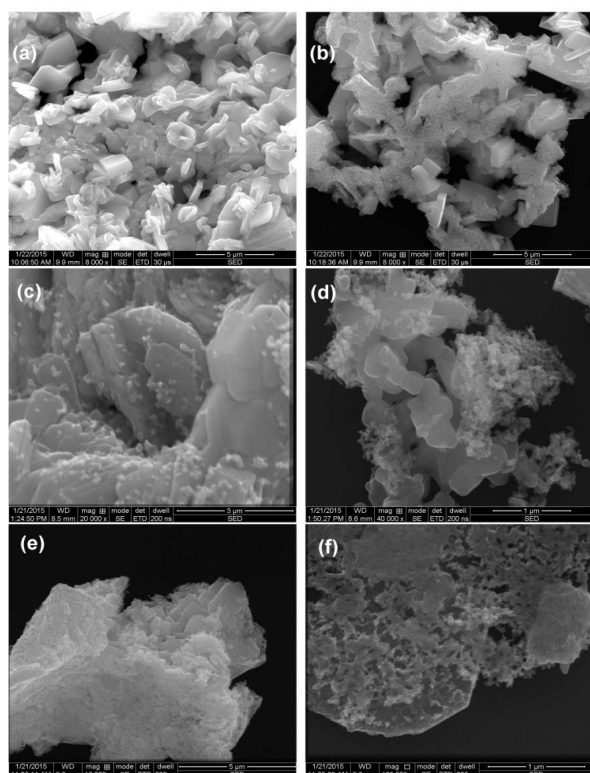
Fig. 3. SEM images of catalyst samples: (a,b) 1CoMoN, (c,d) 3CoMoN, (e,f) 5CoMoN with different magnifications in different areas.

detectable structural changes during nitride formation.[18–21]

Figure 2b displays a bright field image of the MoN sample where one can clearly see an individual nanodomain of γ-Mo$_2$N with an average particles size of 6.5 nm, which is close to crystal size obtained from XRD. Figure 2c displays a selected-area electron diffraction (SAED) pattern of a small representative of γ-Mo$_2$N platelet in a bright field image (Fig. 2b). In the pattern, both spots and rings belong to γ-Mo$_2$N. Spot pattern belongs to the (100) Mo$_2$N zone axis, which means that the platelet was perpendicular to the electron beam. The SAED pattern establishes the characteristic d-lines (111), (200), (220), and (311) for the γ-Mo$_2$N platelet. Figure 2d displays a high-resolution TEM image of a γ-Mo$_2$N platelet with insets showing a selected-area electron diffraction pattern and the measured interlayer planar spacing for {200} orientation of γ-Mo$_2$N, which is in agreement with a reference value.[37]

Figure 3 manifests SEM images of the 1CoMoN, 3CoMoN, and 5CoMoN catalysts with different magnifications in different areas. Figure 3a shows
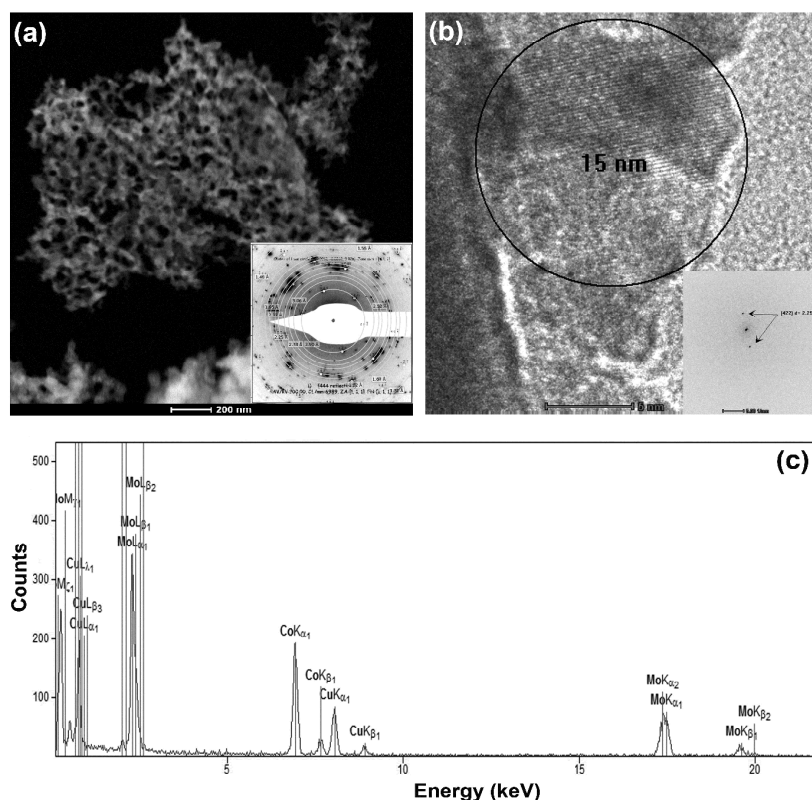
Fig. 4. (a) STEM image of Co$_3$Mo$_3$N in a 3CoMoN catalyst sample with corresponding SAED pattern; (b) HRTEM image of Co$_3$Mo$_3$N with corresponding FFT in the 3CoMoN catalyst; (c) EDX pattern of Co$_3$Mo$_3$N.

ARTICLE   **Journal Name**

that the 1CoMoN sample is a mixture of γ-Mo₂N as major component and MoO₂ platelets. This confirms the increase in amount of the γ-Mo₂N phase in the 1CoMoN catalyst in comparison with the MoN catalyst, in which bigger MoO₂ platelet crystals (Fig.2a) were observed. On the other hand, Figure 3b demonstrates that some part of the 1CoMoN catalyst is having heterogeneous morphology found by STEM-EDX, where some porous microstructure identified as a Co₃Mo₃N phase is uniformly distributed on platelet. On increasing Co loading from 1 to 3 wt.% the Co₃Mo₃N phase also increased and distributed

uniformly over the catalyst that is clearly seen in Figs. 3c and 3d. They show that the Co₃Mo₃N phase is located on γ-Mo₂N platelets. Similarly, by further increase of the Co amount from 3 to 5 wt.%, the particles of Co₃Mo₃N and γ-Mo₂N platelets started to agglomerate. Figs. 3e and 3f disclose Co₃Mo₃N agglomeration located on γ-Mo₂N platelets in the 5CoMoN catalyst. These results are in good agreement with XRD results presented in Table 1, namely, there is almost a two-fold increase in average particle size of the γ-Mo₂N platelets and the Co₃Mo₃N phase on moving from 3CoMoN to 5CoMoN.
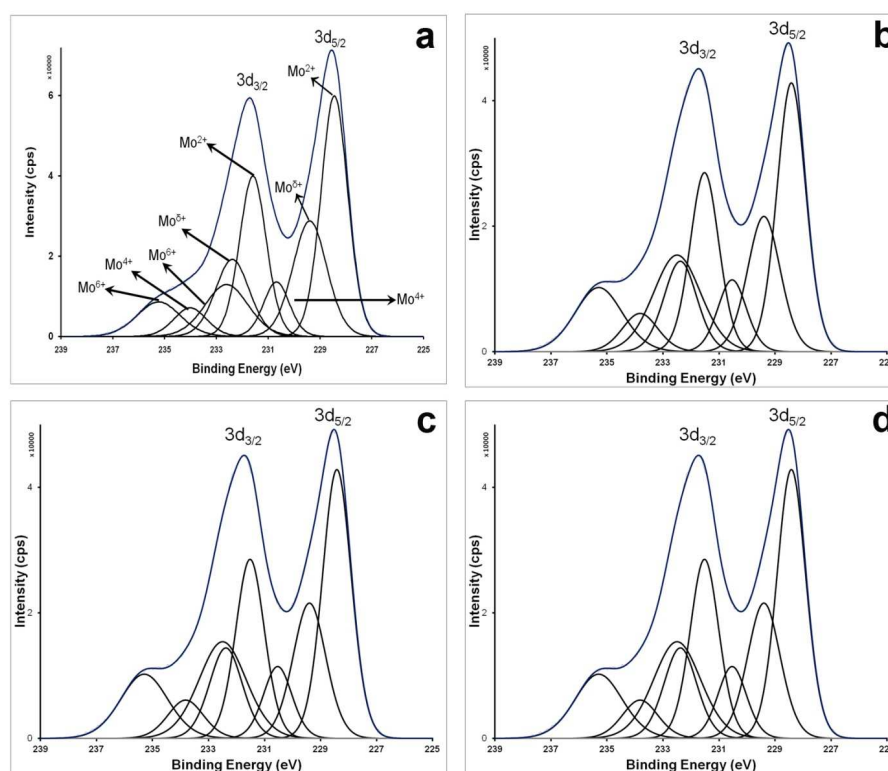
Fig. 5. XPS spectra in Mo 3d region of: (a) MoN catalyst, (b) 1CoMoN catalyst, (c) 3CoMoN catalyst, (d) 5CoMoN catalyst.

Figure 4 displays microscopic images of Co_3Mo_3N in a 3CoMoN catalyst sample and the corresponding EDX pattern. The STEM image in Figure 4a depicts a porous microcrystalline structure of Co_3Mo_3N in the 3CoMoN catalyst. The matching selected area electron diffraction (SAED) clearly establishes the characteristic d-lines 220[3.90Å], 222[3.06Å], 400[2.73Å], 331[2.52Å], 422[2.25Å], 511[2.12Å], 440[1.95Å], and 642[1.48Å] for the Co_3Mo_3N crystal. Investigated Co_3Mo_3N crystals have irregular shape and their average size is about 15 nm (Fig. 4b). The corresponding area live FFT registers the crystalline plane (422) d=2.25 Å. Figure 4c shows STEM-EDX of selected area in Figure 4a, which indicates the presence of cobalt and molybdenum at a Co to Mo ratio of 0.908. This is confirmation for the presence of Co_3Mo_3N phase. TEM and SEM results also confirm that small amounts of cobalt promote γ-Mo_2N formation and prevent γ-Mo_2N and Co_3Mo_3N crystal growth. These results are in good agreement with XRD results presented in Table 1 and Figure 1 indicating that the 5CoMoN catalyst exhibited larger particle sizes of the γ-Mo_2N and Co_3Mo_3N phases in comparison with the rest of catalysts.
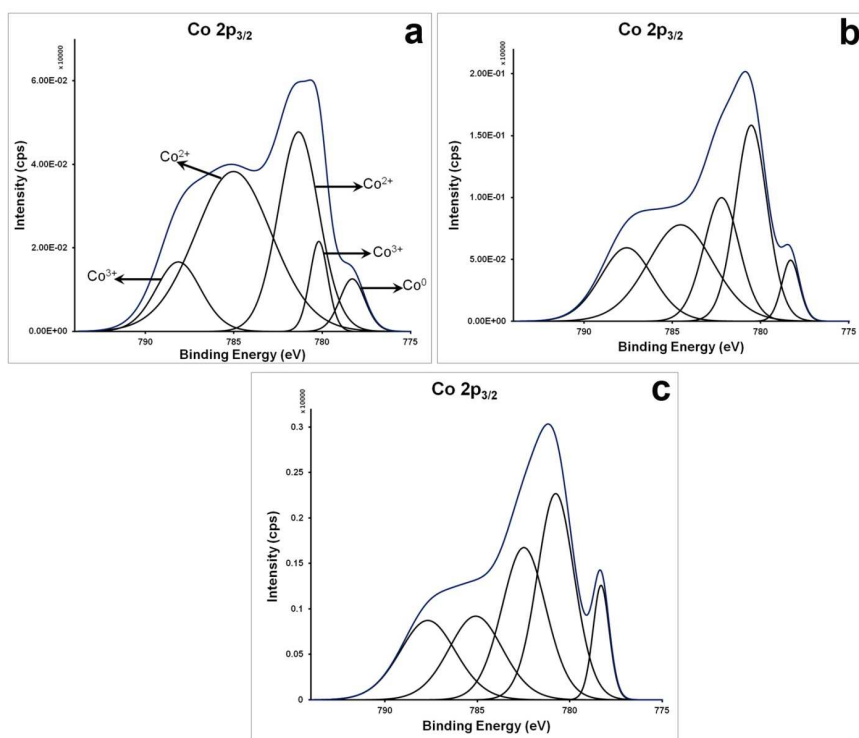
Fig.6. XPS spectra in the Co 2p region: (a) 1CoMoN catalyst, (b) 3CoMoN catalyst, (c) 5CoMoN catalyst.

XPS measurements

Information about molybdenum and cobalt oxidation states distributed over the surface of the studied catalysts can be gained by means of XPS measurements. Figure 5 shows spectra of all catalysts in the Mo 3d region. It is seen in Figure 5a that Mo^{2+} and $Mo^{\delta+}$ are predominant species in MoN samples. Mo^{4+} and Mo^{6+} species in the 3d region are also present. According to Hada et al.[39] Mo^{2+} and $Mo^{\delta+}$ correspond to molybdenum nitride, Mo^{4+} matches to MoO_2, while Mo^{6+} might agree with oxidised form of molybdenum nitride. Introduction of cobalt gave rise to the formation of Co_3Mo_3N. The acquired spectrum is exactly matching with those reported in the literature.[34, 38, 39] Mo^{2+} and $Mo^{\delta+}$ distribution on the surface contributes chiefly to the properties of all catalysts. Typically, metal nitride samples are air sensitive. These samples undergo oxidation during passivation with $1\%O_2/He$. The presence of Mo^{6+} species in XPS is due to oxidized Mo_2N during O_2 passivation.[40]

Figure 6 shows cobalt XPS spectra in the $2p_{3/2}$ region of all catalysts. In the 1CoMoN catalyst, the surface concentration of Co^{2+} is higher than that of other cobalt species, i.e. Co^0 and Co^{3+}. Hada et al.[39] prepared cobalt molybdenum nitride catalysts of various Co content within 0–100%. They reported the maximal Co^0 coverage is observed in catalyst with 30% Co loading. Co^0 species at the surface of catalysts, prepared by this method, are indentified clearly (Figure 6) even at lower Co loadings. Figure 6 manifests an increase of Co^{3+} and Co^0 at the surface on increasing cobalt loading. This is a result of the existence of highly dispersed Co_3Mo_3N species. Hence, citric acid addition during the preparation procedure plays a pivotal role for the formation of highly dispersed Co_3Mo_3N phase.

Catalytic activity

Figure 7 displays results of catalytic activity measurements of MoN, 1CoMoN, 3CoMoN, and 5CoMoN catalysts for ammonia decomposition. It is evident that the MoN catalyst performed a 99% conversion at 600°C. Introduction of cobalt metal during Mo_2N preparation did not change the temperature of 600°C to achieve complete conversion; however, at lower temperatures of 450–550°C the conversion over 1CoMoN is higher than that on MoN catalyst. With the increase of Co loading from 1-3wt.% the increase in conversion reached upto 10% in comparison to that of MoN catalyst. The reason for this difference is associated with formation of Co_3Mo_3N species in the cobalt containing samples. Many authors have reported that, along with $γ-Mo_2N$, Co_3Mo_3N is also active for ammonia decomposition.[29–34] A further increase in Co loading from 3 to 5 wt.% dropped the activity almost equal to that of the MoN catalyst, despite the fact that the latter was less active especially at higher temperatures (over 600°C). This might be due to formation of large crystals of Co_3Mo_3N and $γ-Mo_2N$ platelets in the
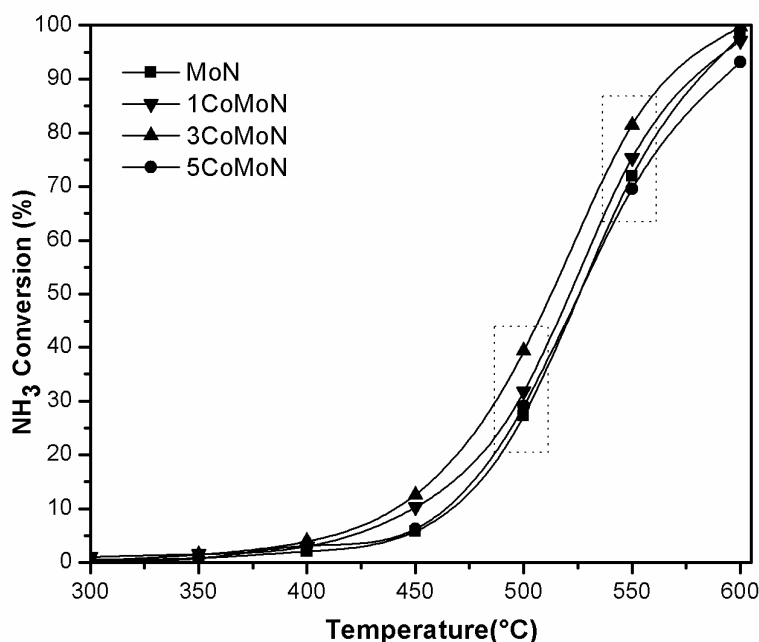
Fig. 7. Catalytic activity of MoN, 1CoMoN, 3CoMoN, and 5CoMoN catalysts
for ammonia decomposition reaction in the temperature range of 300–600°C and GHSV of
6000 h^{-1}.

5CoMoN catalyst. Hada et al. [39] observed the formation of Co$_3$Mo$_3$N structural slab together with different slabs of γ-Mo$_2$N as combined large flat crystallites after the introduction of cobalt at higher loadings in MoN preparation. However, the formation of large flat crystallites was not observed in case of catalysts with low cobalt loading. A similar phenomenon was also observed in the present study. At higher loading (5%) of cobalt agglomeration of Co$_3$Mo$_3$N and γ-Mo$_2$N phases started, which was observed in SEM image (Fig.3e) and XRD results.

Arrhenius plots (Ln(k) *vs* 1/T) for ammonia decomposition are presented in Figure 8 and the obtained activation energies are shown in inset. Bulk MoN catalyst is having the highest activation energy of 131.2 kJ mol^{-1}. Cobalt addition to the catalysts caused a substantial decrease of the activation energy. The activation energy for the 1CoMoN catalyst is 99.74 kJ mol^{-1}, which suggests the promotional effect of cobalt. By increasing Co loading from 1 to 3 wt.% the activation energy still decreased and the 3CoMoN catalyst exhibited the highest activity and the lowest activation energy of 92.8 kJ mol^{-1}. Upon further increase of Co content, the catalytic activity was decreased whereas the activation energy was increased. The 5CoMoN catalyst demonstrated activation energy of 102.6 kJ mol^{-1} owing to the occurrence of Co$_3$Mo$_3$N microstructure coverage on the surface of γ-Mo$_2$N, which leads to an increase in crystal size of γ-Mo$_2$N and Co$_3$Mo$_3$N related to 5% Co loading. The excess
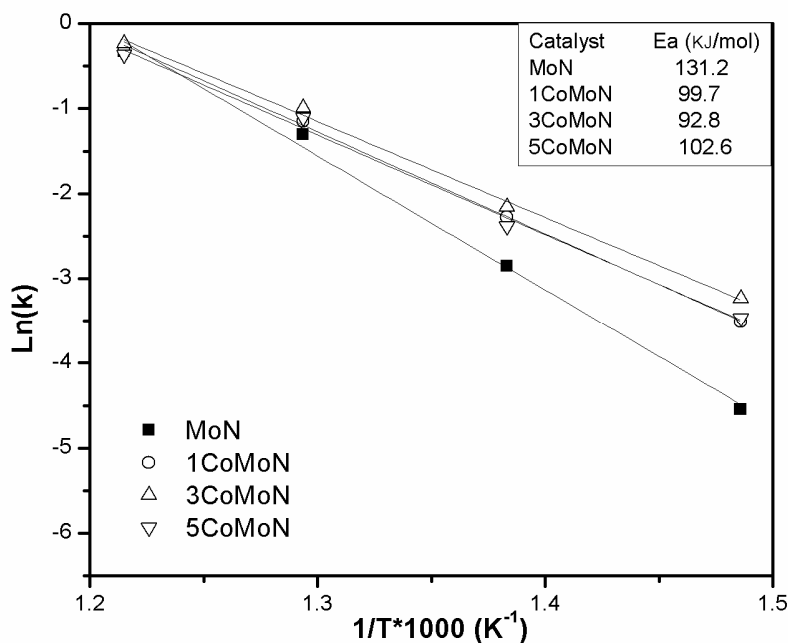
Fig.8: Arrhenius plots for NH_3 decomposition over MoN, 1CoMoN, 3CoMoN and 5CoMoN catalysts.

of cobalt caused an enhanced blocking of the active sites on the surface. Likely, at high Co concentrations few active sites were accessible. Therefore, the beneficial effect of cobalt might arise from enhanced intrinsic activity of the Co_3Mo_3N active sites along increased formation of $\gamma\text{-}Mo_2N$ active sites.

The performances of some ammonia decomposition catalysts are tabulated in Table 2. According to many authors, a 100% ammonia conversion is achieved on applying bulk and supported Mo_2N catalysts at 650°C or higher temperatures.[28,30,36,41] Some other literatures reported that Co-Mo catalysts supported on high surface area supports showed high activity at 600°C. [32,33] In these reports authors characterized the used catalysts and

reported formation of Co_3Mo_3N phase during the ammonia decomposition process, which is responsible for high ammonia decomposition activity. However, it is also known that formation of metal nitride phase will not complete at 600°C. [20,21,34,39] The high activity for these catalysts was mainly due to usage of high Co/Mo ratio and usage of high surface area support to disperse the active phase. For this reason, we chose to study the behaviour of the bulk Co-Mo nitride for ammonia decomposition, since our study has not been reported in the literature for this proposed reaction. Chen et al. [42] studied the conductivity in Co_3Mo_3N and $\gamma\text{-}Mo_2N$ composite material. According to them Co_3Mo_3N / $\gamma\text{-}Mo_2N$ composite material helps to increase the electron carrier density and decrease in resistance. They reported

Journal Name

ARTICLE

that in this composite material Co_3Mo_3N inserted in γ-Mo_2N may lead to distortion of the host lattice and induce the defects in structure and enlarge the constant of crystal lattice of γ-Mo_2N, which not only help in the enhancement of conductivity but also facilitate the charging of the double layer. They also reported high loading of cobalt decreased the conductivity. From this discussion, it is clear that Co_3Mo_3N / γ-Mo_2N composite material is a good electron conductive material. S.F. Yin et al,[3] reported that electron conductive materials are beneficial for ammonia decomposition reaction. Hence these composite materials are showing better activity than their constituents in bulk or supported form. Ammonia conversion at 600°C on all nitride catalysts used in this work manifested higher values than reported conversion values at same temperature. The high catalytic activity of the studied catalysts should be related to the following reasons: (i) formation of Co_3Mo_3N phase at very low   cobalt loadings (ii)

uniform dispersion of Co_3Mo_3N phase on γ-Mo_2N platelets and (iii) good electron conductivity. The stable performance and hydrogen production over the MoN, 1CoMoN, 3CoMoN, and 5CoMoN catalysts are presented in Figure 9. The catalyst stability test was performed at 600°C for 30 h and no deactivation of catalytic performance was observed with all the catalysts at a constant hydrogen production rate.

4. Conclusions

High surface area bulk molybdenum nitride catalysts were successfully synthesised from ammonium heptamolybdate precursor by adding citric acid to the catalyst precursor solutions. By introduction of cobalt, an increase in formation of γ-Mo_2N together with Co_3Mo_3N was observed. The Co_3Mo_3N microstructure was dispersed on γ-Mo_2N platelets. XRD results and SEM images gave evidence that cobalt addition promoted the

Table 2: Catalytic activities of different catalysts for NH_3 decomposition

Catalyst	Metal loading, wt.%	GHSV, h^{-1}	Reaction temperature, °C	NH_3 conversion, %	Reference
Ru/CNT	5	30 000	500	100	[7]
CoMo/γ-Al_2O_3	5	36 000	600	99.0	[32]
Co_7Mo_3/MCM-41	5	36 000	600	99.2	[33]
MoN_x/α-Al_2O_3	12	3 600	600	75.2	[39]
MoN_x/SBA-15	12	15 800	650	100	[28]
Co_3Mo_3N/Mg(Al)O	10	7 600	600	–	[29]
$CoMoN_2$/CNT	10	11 000	600	71.5	[30]
La-$CoMoN_2$/CNT	10	11 000	600	97.6	[30]
Mo_2C	bulk	36 000	600	71.0	[31]
Mo_2N	bulk	15 000	600	70.1	[41]
MoN	bulk	6 000	600	97.2	this work
3CoMoN	bulk	6 000	600	98.3	this work
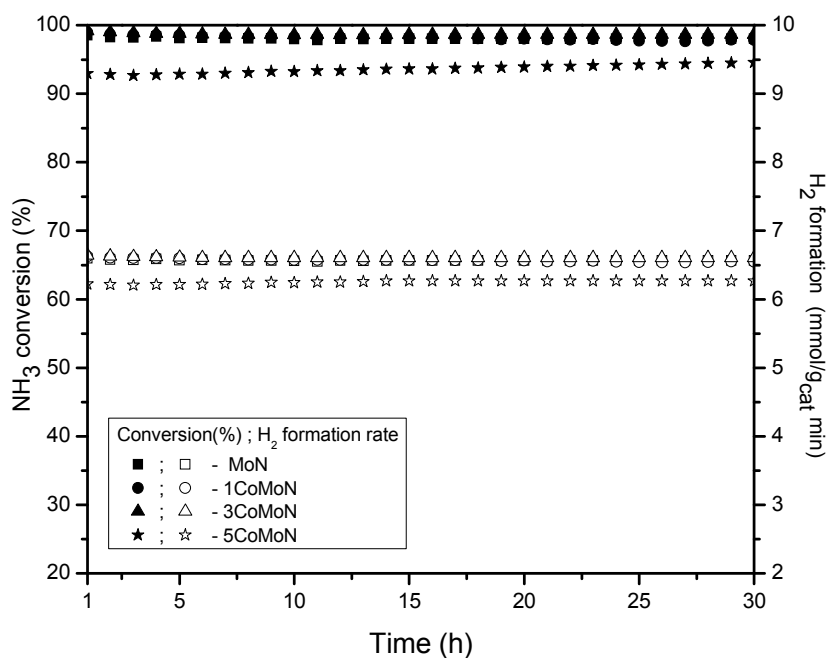
Fig.9. Stability performance and hydrogen productivity over MoN, 1CoMoN, 3CoMoN, and 5CoMoN catalysts at 600°C and GHSV of 6000 h^{-1}.

formation of γ-Mo$_2$N. Hence, citric acid as chelating agent promotes mono and bimetallic compounds, which further helps in formation of mono and bimetallic nitrides. The effect of cobalt loading was optimised and it was found that 3 wt.% Co is a suitable concentration to form uniformly dispersed γ-Mo$_2$N and Co$_3$Mo$_3$N. Higher cobalt loadings led to agglomeration of γ-Mo$_2$N and Co$_3$Mo$_3$N, which caused drastic deactivation for ammonia decomposition. Among all unsupported catalysts, 3CoMoN samples exhibited the highest catalytic activity. Hence, 3 wt.% is an optimal cobalt loading in MoN preparation for higher activity.

Acknowledgement

References

1. H. Danielle, G. V. Dionisios and G. C. Jingguang, *Nature Chem.*, 2010, **2**, 484–489.

2. A. S. Chellappa, C. M. Fischer and W. J. Thomson, *Appl. Catal. A-Gen.*, 2002, **227**, 231–240.

3. S. F. Yin, B. Q. Xu, X. P. Zhou and C. T. Au, *Appl. Catal. A-Gen.*, 2004, **277**, 1–9.

4. F. Schuth, R. Palkovits, R. Schlogl and D. S. Su, *Energy Environ. Sci.,* 2012, **5**, 6278–6289.

5. E. García-Bordejé, S. Armenise and L. Roldán, *Catal. Rev.,* 2014, **56,** 220–237.

6. X. Duan, J. Ji, G. Qian, X. Zhou, D. Chen, *Catal. Today.,* 2015,**249**,2–11.

7. S. F. Yin, Q. H. Zhang, B. Q. Xu, W. X. Zhu, C. F. Ng and C. T. Au, *J. Catal.*, 2004,**224**,384-396.

8. S.F. Yin, B.Q. Xu, S.J. Wang, C.F. Ng and C.T. Au, *Catal. Lett.,* 2004, **3–4**,113-116.

9. X. Duan, J. Zhou, G. Qian, P. Li, X. Zhou and D. Chen, *Chin J Catal*, 2010, **31**, 979–986.

10. P. M. Patterson, T. K. Das and B. H. Davis, *Appl. Catal. A-Gen.*, 2003, **251**, 449–455.

11. L. Leclercq, M. Provost, H. Pastor and G. Leclercq, *J. Catal.*, 1989, **117**, 384–395.

12. J. B. Claridge, A. P. E. York, A. J. Brungs, C. Marquez-Alvarez, J. Sloan, S. C. Tsang and M. L. H. Green, *J. Catal.*, 1998,**180**, 85–100.

13. R. Schlögl, in Handbook of Heterogeneous Catalysis; G. Ertl, H. Knözinger, F. Schüth, *J. Weitkamp, Eds*., Wiley-VCH, Weinheim, 2008.

14. A. Boisen, S. Dahl, J. K. Nørskov, C. H. Christensen, *J.Catal.*, 2005, **230**, 309-312.

15. X. Duan, J. Ji, G. Qian, C. Fan, Y. Zhu, X. Zhou, D. Chen, W. Yuan, *J. Mol. Catal. A Chem.*, 2012, **357,** 81-86.

16. D. A. Hansgen, D. G. Vlachos and J. G. Chen, *Nature Chem.,* 2010, **2**, 484-489.

17. L. Volpe and M. Boudart, *Science*, 1973, **181**, 547–549.

18. L. Volpe and M. Boudart, *J. Solid State Chem.*, 1985, **59**,332–347.

19. D. Mckay, J. S. J. Hargreaves, J. L. Rico, J. L. Rivera and X.L. Sun, *J. Solid State Chem.*, 2008, **181**,325–333.

20. J.G. Choi, R. L. Curl and L. T. Thompson, *J. Catal.*, 1994, **146,**218–227.

21. C. H. Jaggers, J. N. Michaels and A. M. Stacy, *Chem. Mater.*,1990, **2**,150–157.

22. C. J. H. Jacobsen, S. Dahl, B. S. Clausen, S. Bahn, A. Logadottir and J. K. Norskov, *J. Am. Chem. Soc.*, 2001, **123**, 8404–8405.

23. R. Kojima and K. I. Aika, *Appl. Catal. A-Gen.*, 2001, **215**, 149–160.

24. R. Kojima and K. I. Aika, *Appl. Catal. A-Gen.*, 2001, **218**, 121–128.

25. C. J. H. Jacobsen, M. Brorson, T. Sehested, H. Teunissen and E. Turnqvist, *US Patent* 1999, **6235676**.

26. C. J. H. Jacobsen, *Chem. Commun.*, 2000,**12**, 1057–1058.

27. C.S. Lu, X. N. Li, Y. F. Zhu, H. Z. Liu and C. H. Zhou, *Chin. Chem. Lett.*, 2004, **15**,105–108.

28. H. Liu, H. Wang, J. Shen, Y. Sun, and Z. Liu, *J. Nat. Gas Chem.*, 2006, **15**, 178–180.

29. Y. Xiang and X. Li, *Chin. J. Chem. Eng.*, 2005, **13**, 696–700.

30. Z. Zhao, H. Zou, W. Lin, *J. Rare Earths*, 2013, **31**,247–250.

31. Z. Weiqing, P. C. Thomas, K. Payam, J. Timo, F. Benjamin, S. Klaus, Z. Wei, S. D. Sheng, S. Ferdi and S. Robert, *J. Am. Chem. Soc.*,2013, **135**, 3458–3464.

32. J.Ji, X. Duan, G. Qian, X. Zhou,G. Tong, W. Yuan, *Int. J. Hydrogen Energy* 2014, **39**, 12490-12498.

33. X. Duan, G. Qian, X. Zhou, D. Chen, W. Yuan, *Chem. Eng*. J. 2012, **207-208,** 103-108.

34. K. Hada, J. Tanabe, S. Omi and M. Nagai, *J. Catal.*, 2002, **207**, 10–22.

35. A.V. Pashigreva, O.V. Klimov, G.A. Bukhtiyarova, M.A. Fedotov, D.I. Kochubey, Yu.A. Chesalov, V.I. Zaikovskii, I.P. Prosvirin and A.S. Noskov, *Stud. Surf. Sci. Catal.* 2010, **175**,109-116.

36. V. Tagliazucca, M. Leoni and C. Weidenthaler, *Phys. Chem. Chem. Phys.,* 2014, 16, 6182–6188.

37. W. F. McClune, Ed., *Powder Diffraction File, Inorganic Compounds, JCPOS,* pattern 25-1366, Swarthmore, 1980.

38. Z. Kejun, Z. Lixue, C. Xiao, H. Xiang, W. Xiaogang, D. Shanmu, H. Pengxian, Z. Chuanjian, W. Shan, G. Lin and C. Guanglei, *J. Phys. Chem. C*, 2013, **117**, 858–865.

39. K. Hada, M. Nagai and S. Omi, *J. Phys. Chem. B*, 2001, **105**, 4084–4093.

40. R.N. Panda and S. Kaskel, *J. Mater. Sci.,* 2006, **41**, 2465-2470.

41. C. Liang, W. Li, Z. Wei, Q. Xin and C. Li, *Ind. Eng. Chem. Res.*, 2000, **39**, 3694–3697.

42. C. Chen, D. Zhao, D. Xu and X. Wang, Mater. *Chem. and Phys.,* 2006, **95**, 84–88.

Hydrogen production by ammonia decomposition using high surface area Mo$_2$N and Co$_3$Mo$_3$N catalysts

Seetharamulu Podila[a], Sharif F. Zaman[ab]*, Hafedh Driss[b], Yahia A. Alhamed[a,b], Abdulrahim A. Al-Zahrania [b], Lachezar A. Petrov[a]